V European Conference on Computational Fluid Dynamics
ECCOMAS CFD 2010
J. C. F. Pereira and A. Sequeira (Eds)
Lisbon, Portugal, 14–17 June 2010

VISCOUS FLOW AROUND TWO BODIES IN RELATIVE MOTION

F.Mahdavi Zafarghandi [*], S.M.H.Karimian [†], and S.Noori[††]

[*,†] Center of Excellence in Computational Aerospace Engineering
Aerospace Engineering Department, Amirkabir University of Technology, Tehran, Iran
e-mail: f_mahdavi1198@yahoo.com
e-mail: hkarim@aut.ac.ir

[††]Aerospace Research Institute, Ministry of Science, Research and Technology, Tehran, Iran
s_noori@aut.ac.ir

Key words: Turbulent Flow, Compressible flow, Moving grid, Relative motion

Abstract. *An efficient dual time implicit approach is used to solve viscous turbulent flow around two bodies with general motion. The grid includes a background grid and two sets of grids around the moving bodies. Rotational and translational motions of two bodies are managed separately in this grid arrangement. In this paper the overset concept for hybrid grid is used and flow variables are interpolated with a simple method. An implicit dual time stepping method is used to discretize the unsteady two dimensional Navier-Stokes equations.* $k-\varepsilon$ *model is employed for turbulence modeling. To accelerate convergence, the local pseudo-time stepping and implicit residual averaging are applied. Comparison of results with the experimental and numerical data, show good agreement with both sources.*

1 INTRODUCTION

Nowadays simulation of unsteady compressible flow around moving bodies can be found in aerospace literature. Since the solution domain changes continuously in moving body problems, special care should be paid to retain the quality of grid. The simplest method for a moving boundary flow problem is to regenerate grid around the body after each step of its motion. Although this approach is desirable for structured grids [1], but it is a time consuming process. The other method is based on dynamic mesh [2-4]. In this approach the computational grid deforms locally by using a spring-analogy type algorithm. This approach is a time consuming process because of repeating process. For large motions overset grid can be used [5-7]. In this method each body has its own grid. On each grid, chimera holes are defined in regions where the grid overlaps solid bodies belonging to the other grids. Advantage of chimera grid is simulation of several moving bodies with high quality grid around each of them. The disadvantage of it, is the large number of interpolations which is required in this method. The other method is using hybrid grids in moving boundary problems [8-11]. In this approach, solution domain is divided into three zones. As it seen in the next section, general motion of a single body can be simulated easily with these three zones. The advantage of this approach is that the number of node deletion/insertion process is minimized to almost nothing. Even in large translational displacements only a few elements merge together.

This method was used by Ref.10 to simulate the rotational/oscillational motion of a two-dimensional body. For the solution of unsteady Navier-Stokes equations they used upstream splitting method of AUSM [12]. Later on Alisadeghi et al modified the method of Ref.10 to provide a smoother grid movement in the solution domain. They solved unsteady viscous flow around a single body in motion. Extension of the work of Ref.11 to inviscid flow simulation of two bodies in motion with respect to each other was carried out by Salehi et al [13]. In the present work, the method of Ref.13 is generalized for the solution of viscous turbulent flow around two bodies in relative motion with respect to each other. For this purpose boundary conditions of Refs [11&13] are modified as well.

Governing equation of viscous turbulent flow are solved using implicit dual time stepping scheme of Refs. [4 &14]. An explicit Runge-Kutta multistage scheme is applied for iterating the solution in pseudo time in each time step. Convergence acceleration is increased with local pseudo-time stepping and implicit residual averaging [15]. Finally computational results are compared with experimental data. Also to demonstrate correct performance of the present method different benchmark problems, defined in this paper, are solved.

2 GRID CONFIGURATION

The general motion of a moving body is a combination of translational and rotational motions therefore the subdivision of solution domain is divided into three zones. The third zone, as shown in Fig.1a, is a background Cartesian grid that is generated in solution domain.

In addition to the background grid, around body A two other zones of grids are generated. The first zone is body A and the surrounding grid fixed to the body and moves with it, and the second zone has a squared boundary and contains the grid surrounding the first zone. In translational motion of body A first and second zones will translate with the body but in rotational motion only the first zone will rotate with the body A. The background grid and these two surrounding grids are called grid A. So in

this way, general motion of body A will be simulated with the least node deletion/insertion and interpolation.

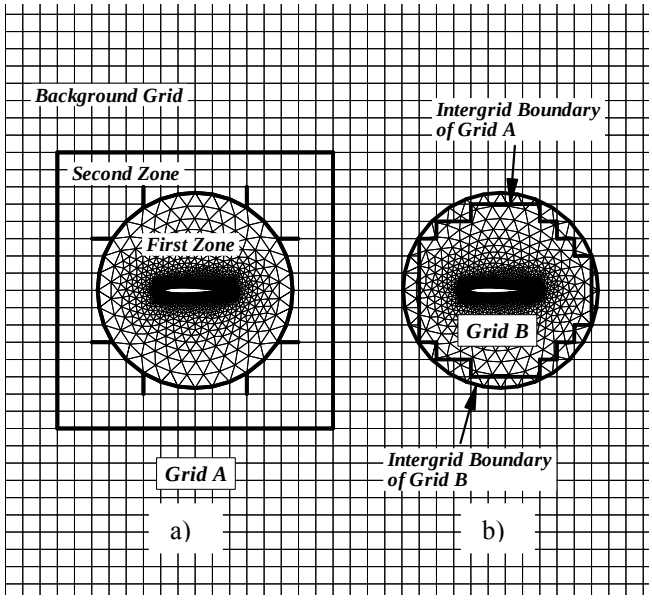

Fig 1. Grid configuration surrounding body A and B.

The body B will have only rotational motion so any type of grid (structured, unstructured or hybrid grid) can be generated around it. As shown in Fig.1a triangular unstructured gird with a circular boundary is generated around it in this study; this grid is called grid B. Grid B is overset on the background grid. In the present study, solution strategy is solving the flow field on two sets of grids A and B, separately. In the process of flow solution on grid A, the regions of intergrid boundary of grid A is excluded from the solution domain. So the values of this region are interpolated from the previous solution done on grid B and the boundary values on the intergrid boundary of grid B are interpolated from the solution previously calculated on grid A. For more details about grid generation approach and overset implementations see Ref. 13

3 SOLUTION ALGORITHEM

The two dimensional unsteady compressible Navier-Stokes equations in the Cartesian coordinate system

$$\frac{\partial}{\partial t}\iint_{\Omega} w\,dx\,dy + \oint_{\partial\Omega}((F^i - F^v)\,dy - (G^i - G^v)\,dx) = 0 \qquad (1)$$

where $w=(\rho,\rho u,\rho v,E)$ is the vector of conserved quantities, F^i and G^i represent the convective fluxes and F^v and G^v describe the diffusion fluxes as following:

$$F^i = \begin{pmatrix} \rho u_r \\ \rho u_r u + P \\ \rho u_r v \\ (\rho E + p)u_r + u_m P \end{pmatrix}, \quad G^i = \begin{pmatrix} \rho v_r \\ \rho v_r u \\ \rho v_r v + P \\ (\rho E + p)v_r + v_m P \end{pmatrix}$$
$$F^v = \begin{pmatrix} 0 \\ \tau_{xx} \\ \tau_{xy} \\ u\tau_{xx} + v\tau_{xy} + q_x \end{pmatrix}, \quad G^v = \begin{pmatrix} 0 \\ \tau_{yx} \\ \tau_{yy} \\ u\tau_{xy} + v\tau_{yy} + q_y \end{pmatrix} \qquad (2)$$

where ρ, P, u, v, u_r, v_r and E denote density, pressure, Cartesian velocity components, relative velocities and total energy, respectively. The relative velocities are defined as

$$u_r = u - u_m, \quad v_r = v - v_m \qquad (3)$$

where u_m and v_m are the Cartesian velocity components of control-volume boundary. τ_{xx}, τ_{xy} and τ_{yy} are the stress tensors and q_x, q_y are the heat flux vector components. The viscosity coefficient μ, is calculated according to Sutherland's law. The equation (1) are augmented by the equation of state, which for a perfect gas is given by,

$$P = (\gamma - 1)\rho\left[E - \frac{u^2 + v^2}{2}\right] \qquad (4)$$

For turbulent modeling, a two-equation $k-\varepsilon$ model is used. The turbulent transport equations can be written in form of mean flow equation (1).

$$\frac{\partial}{\partial t}\iint_\Omega w_t \, dx\, dy + \oint_{\partial\Omega}((F_t^i - F_t^v)\, dy - (G_t^i - G_t^v)\, dx) = \iint_\Omega S_t dx dy \qquad (5)$$

Where $w_t = (\rho k, \rho\varepsilon)$, F_t^i, G_t^i represent the turbulent convective fluxes and F_t^v, G_t^v describe the effect of turbulent viscous diffusion. The source term S_t describes production and dissipation of turbulence quantities. The turbulent eddy viscosity is calculated from:

$$\mu_t = C_\mu \rho \frac{k^2}{\varepsilon} \qquad (6)$$

In this work, the turbulence equations are solved with the main flow equations in a fully-coupled manner. Equation (1) is applied to each control volumes with area of A_i and can be written as

$$\frac{d}{dt}(w_i A_i) + R_i(w) - D_i(w) = 0 \qquad (7)$$

Where $R_i(w)$ is the sum of the convective fluxes and viscous fluxes in x and y directions and $D_i(w)$ is the numerical dissipative term [16] which is added to Eq. (1). This $D_i(w)$ is combined with fourth and second differences with coefficients that depend on the local pressure gradient. This term is introduced in Ref.16.

A fully implicit time discretisation (in real time) of Eq. (7) can be written as: [17]

$$\frac{d}{dt}(w_i^{n+1} A_i^{n+1}) + R_i(w^{n+1}) - D_i(w^{n+1}) = 0 \qquad (8)$$

In this paper a second order accurate Backward Difference Formula [18] is used as follows

$$\frac{3}{2\Delta t}(w_i^{n+1} A_i^{n+1}) - \frac{2}{\Delta t}(w_i^n A_i^n) + \frac{1}{2\Delta t}(w_i^{n-1} A_i^{n-1}) + R_i(w^{n+1}) - D_i(w^{n+1}) = 0 \qquad (9)$$

A Dual Time Stepping metod is used to solve the coupled nonlinear equations (9) at each time step [18]. This can be done with the solution of the following equation.

$$\frac{\partial w}{\partial \tau} + R^*(w^n) = 0 \qquad (10)$$

τ is pseudo-time in each time step, and $R^*(w^n)$ is the unsteady residual given by

$$R^*(w^n) = \frac{3}{2\Delta t}(w_i^{n+1}A_i^{n+1}) - \frac{2}{\Delta t}(w_i^n A_i^n) + \frac{1}{2\Delta t}(w_i^{n-1}A_i^{n-1}) + R_i(w^{n+1}) - D_i(w^{n+1}) \quad (11)$$

Equation (10) is a modified steady state problem in pseudo-time and is solved by using explicit Runge-Kutta multistage method. To accelerate convergence, local pseudo-time stepping and implicit residual averaging are used. The four-stage Runge-Kutta scheme is given by,

$$\begin{aligned}
w^{(0)} &= (w_i^{n+1})^m \\
w^{(1)} &= w^{(0)} - \frac{1}{4}\frac{\Delta\tau}{A_i} R_i{}^*(w^{(0)}) \\
w^{(2)} &= w^{(0)} - \frac{1}{3}\frac{\Delta\tau}{A_i} R_i{}^*(w^{(1)}) \\
w^{(3)} &= w^{(0)} - \frac{1}{2}\frac{\Delta\tau}{A_i} R_i{}^*(w^{(2)}) \\
w^{(4)} &= w^{(0)} - \frac{\Delta\tau}{A_i} R_i{}^*(w^{(3)}) \\
(w_i^{n+1})^{m+1} &= w^{(4)}
\end{aligned} \qquad (12)$$

where

$$R^*(w^{(1)}) = \frac{3}{2\Delta t}(w_i^{(1)}A_i^{n+1}) - \frac{2}{\Delta t}(w_i^n A_i^n) + \frac{1}{2\Delta t}(w_i^{n-1}A_i^{n-1}) + R_i(w^{(1)}) - D_i(w^{n+1}) \qquad (13)$$

n and m are real and pseudo time stages respectively.

With the numerical dissipative term in the first stage of Eq. (13) computational efficiency will increase. The pseudo-time step for each cell which is limited by stability considerations is given as

$$\Delta\tau_i = \min\left(\frac{CFL\ A_i}{\sum_{j=1}^{N}\lambda_j}, \frac{2\Delta t}{3}\right) \qquad (14)$$

where j denotes edge of the corresponding cell, and

$$\lambda = u\Delta y - v\Delta x \qquad (15)$$

For accelerating convergence, the local pseudo time stepping and residual smoothing are used in this paper. The real time step can be chosen based on accuracy considerations.

At the far field, non-reflecting boundary conditions are used based on the characteristic analysis. At the solid wall boundary, the no-slip condition needs to be imposed. For satisfying no-slip condition in unsteady flow, the particles of fluid just above the surface of airfoil move with the airfoil speed. The pressure value at the solid wall is calculated by extrapolating from the values of adjacent cells. The wall function conditions are also considered for near wall turbulent calculations.

4 OVERSET IMPLEMENTATION

As mentioned earlier, governing equations are solved on two sets of grids iteratively. At each time step, the system of equations are solved on grid A which has outer flow boundary and its own intergrid boundary, as shown in Fig.1. For this purpose boundary conditions on intergrid boundary A are interpolated from the most updated values flow variables on grid B. From these results on grid A, flow variables along the intergrid boundary B are interpolated to provide boundary conditions for the solution of flow field on grid B. After the solution of flow field on grid B, the same process can be

repeated until the error between intergrid boundary values of two successive iterations for both grids A and B becomes less than a desired value

5 NUMERICAL RESULTS

In this section the capability of the present method for the simulation of fluid flow over moving body are evaluated. The method is validated by comparison of its result with experimental data and other numerical results.

In order to verify the solution algorithm on two sets of grids as described before, the turbulent steady state flow with Mach 0.729, Re=6,500,000 at 2.79degrees angle of attack over RAE 2822 airfoil is considered on two different grid configurations. The airfoil is set in grid A and grid B is clean. Grid configurations shown in Fig.2 are, a) clean grid close to body A, and b) clean grid far from body A. In Fig.2 a grid B is close to grid A, forming an overlapping region. In Fig. 3b, however grid B is far from grid A and no overlapping region is formed.

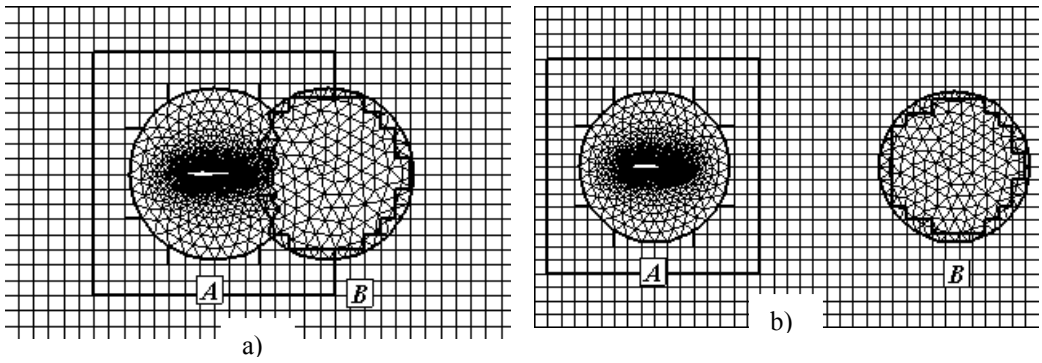

Fig 2. a) clean grid close to body A, and b) clean grid far from body A

Fig.3 shows the grid configuration around RAE 2822. Figs.4 and 5 illustrate the comparison of pressure coefficient distribution and surface force coefficient distribution on the surface of airfoil with the experimental data [19]. Results obtained on both grids are in excellent agreement with each other and with experimental data.

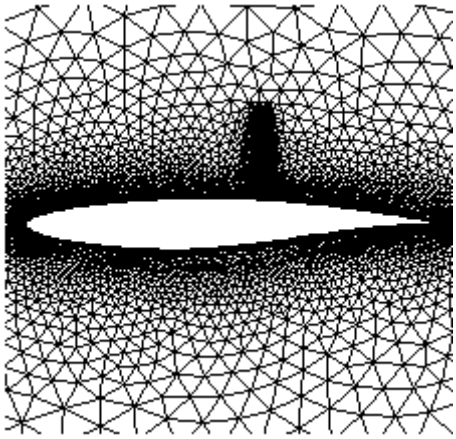

Fig 3. Grid configuration surrounding airfoil RAE 2822

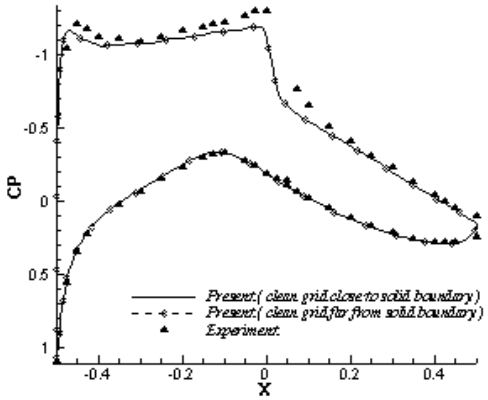

Fig 4. Comparison of surface pressure coefficient distribution ; present results and experimental data; airfoil RAE 2822 at M= 0.729,Re=6500000,α=2.79º

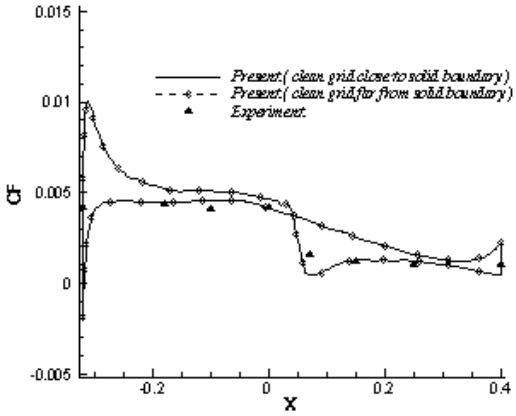

Fig 5. Comparison of surface force coefficient distribution; present results and experimental data; airfoil RAE 2822 at M= 0.729, Re=6500000,α=2.79º

Again to demonstrate that the solution strategy is independent from the grid arrangement and also the accuracy of interpolation stencil used in the overlapping layer, flow field of 1st test case is solved on two different grids shown in Fig.6. These include, a) body set in grid A and grid B is clean, and b) body is set in grid B and grid A is clean.

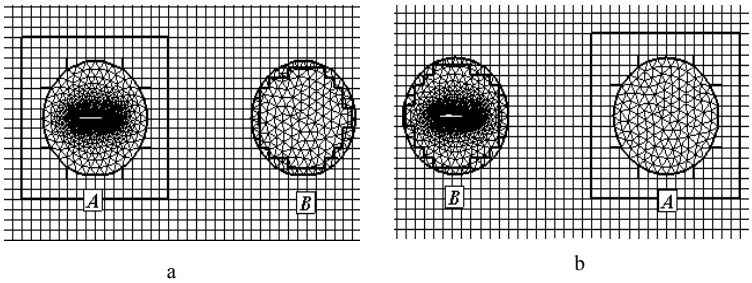

Fig 6. a) Body A and clean grid B, and b) Body B and clean grid A

Fig.7 shows the comparison of surface pressure coefficient distribution on two grids with each other and with experimental data [19]. Same comparison is made for surface

force coefficient distribution in Fig.8. Again results obtained on two grids are in excellent agreement with each other.

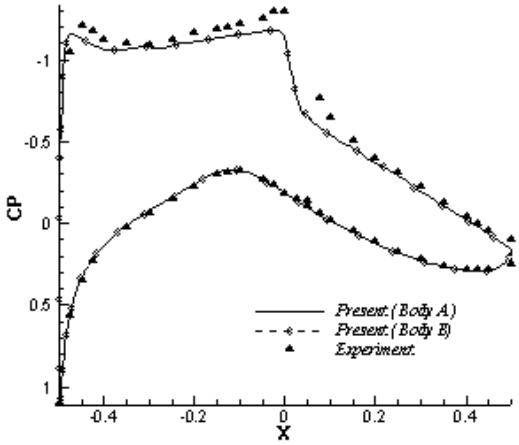

Fig 7. Comparison of surface pressure coefficient distribution; present results and experimental data; airfoil RAE 2822 at M= 0.729, Re=6500000, α=2.79º

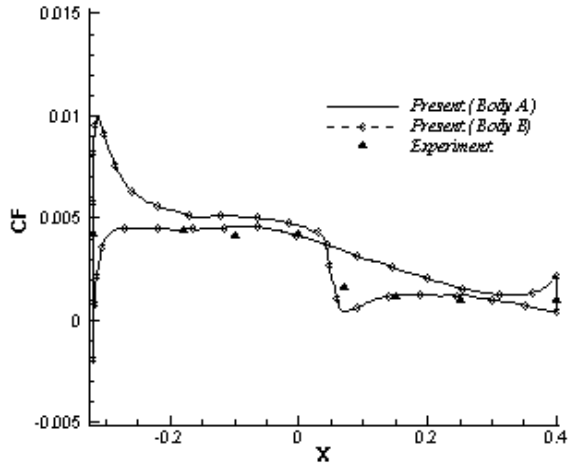

Fig. 8 Comparison of surface force coefficient distribution; present results and experimental data; airfoil RAE 2822 at M= 0.729, Re=6500000, α=2.79º

Fig.9 illustrates turbulent kinetic energy around airfoil. As shown in Fig.9 the disturbance of flow behind shock have increased in upper surface of airfoil because of reversed pressure gradient resulting of shock.

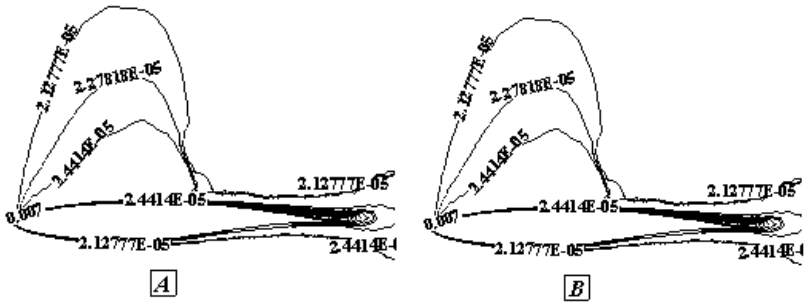

Fig 9. Turbulent kinetic energy around airfoil a) Body A, and b) Body B

In third case, steady state flow at Mach 0.75, Re=6200000 and α=2.81º for RAE 2822 are solved on the grids of Fig.6. Comparison of pressure coefficient distribution obtained on these two grids with each other and with the experimental data [19] is shown in Fig.10. Same comparison is shown for surface force coefficient distribution in Fig.11. Results of the present study agree very well with each other and with experimental data.

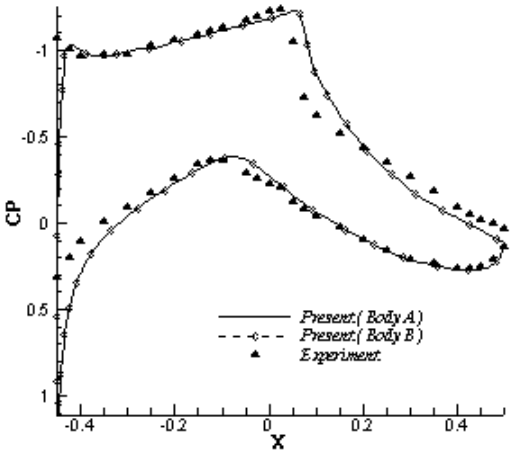

Fig 10. Comparison of surface pressure coefficient distribution; present results and experimental data; airfoil RAE 2822 at M= 0.75, Re=6200000, α=2.81º

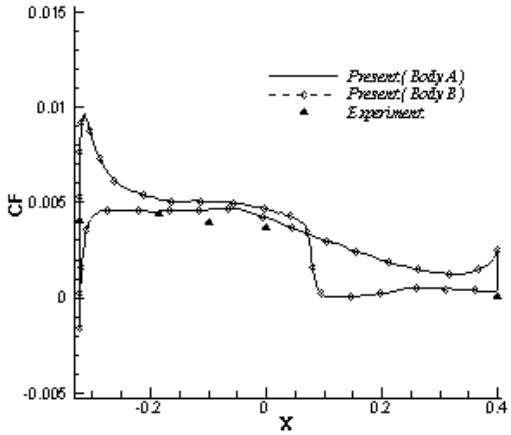

Fig 11. Comparison of surface force coefficient distribution; present results and experimental data; airfoil RAE 2822 at M= 0.75, Re=6200000, α=2.81

Fig.12 shows the contours of Mach and produced shock in upper surface of airfoil.

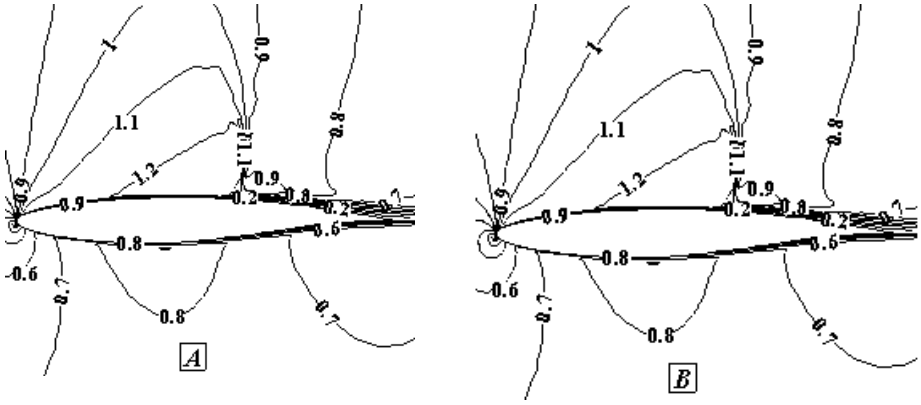

Fig 12. Mach contours and shock wave a) Body A, and b) Body B

As the forth test case, we would like to solve the unsteady flow over the oscillatory pitching airfoil of NACA 0012, defined in AGARD CT5 test case [20], which has been widely studied in the literature. Grids of Fig 2 are used for the simulation of unsteady flow of CT5. Consider the harmonic pitching motion of airfoil about the quarter chord of it with the following time dependent varying angle of attack,

$$\alpha = \alpha_m + \alpha_0 \sin \omega t$$

Where α_m is the mean angle of attack, α_0 is the amplitude of its oscillation, and ω is the angular frequency of the motion, related to reduced frequency, *k,* by

$$k = \frac{\omega c}{2U_\infty}$$

In this relation, U_∞ is the free stream velocity and c is the chord length of the airfoil. Flow conditions are

$$M_\infty = 0.755,\ \alpha_m = 0.016,\ \alpha_0 = 2.51,\ k = 0.0814,\ \mathrm{Re} = 5.5 \times 10^6$$

The above problem is solved on two different grids shown in Fig.2. As shown in Fig.2 a, the oscillating airfoil would be within the grid A. Grid B is close to grid A, forming an overlapping region. In Fig.3b, however the oscillating airfoil is set within grid A. Grid B is far from grid A and no overlapping region exists.

Numerical calculation of unsteady flow is started from the steady state solution of Mach 0.755 with Re=5500000 flow over NACA 0012 airfoil at 0.016 degrees angle of attack on both grids. The variation of normal force coefficient obtained from the present method on both grids is compared with experimental data in Fig.13. Results obtained on both grids are in excellent agreement with each other. In addition to this, results of the present study agree very well with the results of experiment [20]. The difference between numerical results and experimental data observed here has been reported by other researchers in the literature, as well [9& 21]. This difference can be eliminated if α_m is changed slightly.

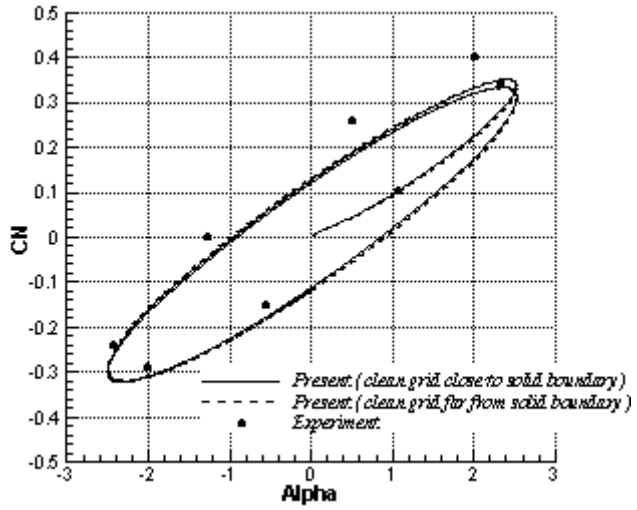

Fig 13. Comparison of normal-force coefficient loop; present results and experimental data, AGARD CT5 test case; airfoil NACA 0012

Once again to demonstrate grid configuration independency of the algorithm in a moving body problem, CT5 test case is solved on grids of Fig.6. The variations of normal force coefficient obtained from the present method on both grids are compared with the experimental data in Fig. 14. Results obtained on both grids are in excellent agreement with each other, and with the experimental data

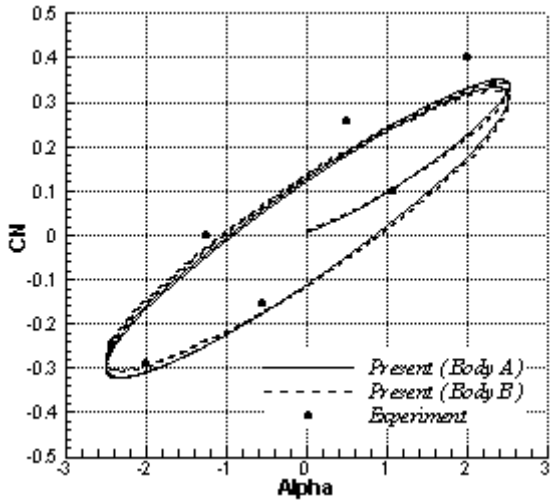

Fig 14. Comparison of normal-force coefficient loop; present results and experimental data, AGARD CT5 test case; airfoil NACA 0012

For translational-rotational motion, the fifth test case is defined. Two cases with the same physics of flow field are considered, in Fig.15. Two NACA0012 airfoils are located at a distance equal to 140 chords from each other. In the first case, the left airfoil is stationary and the oscillating airfoil at the right moves toward the left with Mach 0.5 in a stationary air. In the second case, the airfoil at the left and the air move together

with Mach 0.5 and Re=10,000 toward the stationary oscillating airfoil at the right. Parameters governing the oscillating airfoil are $\alpha_m = 0,\ \alpha_0 = 2.51,\ k = 0.0814$. Unsteady solution is obtained using local pseudo time steps, and real time step of 2.55E-2 s. Lift and drag coefficient histories of the right airfoil in both cases are compared with each other in Figs.16 and 17. The excellent agreement shows the accuracy of the algorithm for simulation of unsteady problems. The little difference between the two results is due to the differences between the grids generated around the right airfoil in two cases.

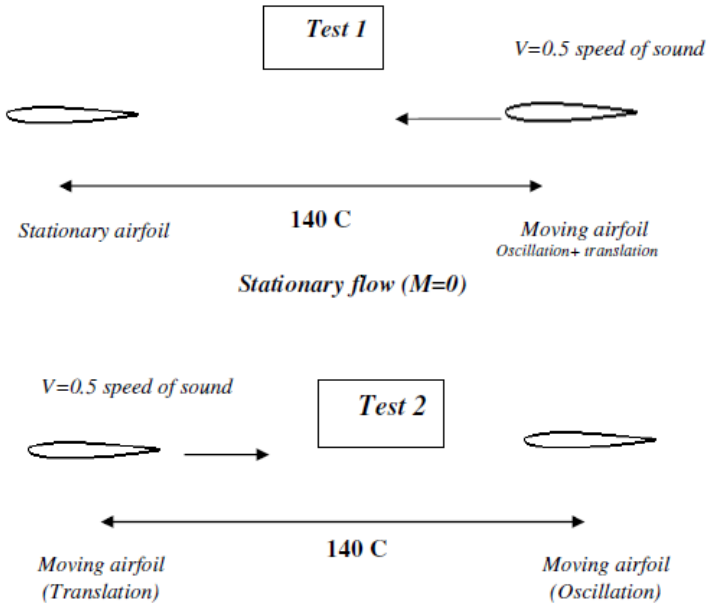

Fig 15. Illustration of test definition for rotational-translational motion of two bodies with respect to each other

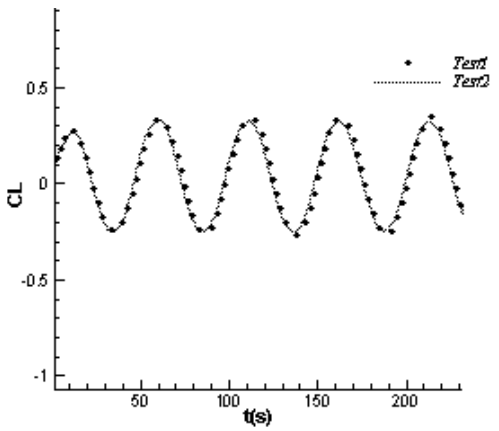

Fig 16. Lift coefficient history of NACA0012 airfoil for rotational- translational motion, cases 1 and 2

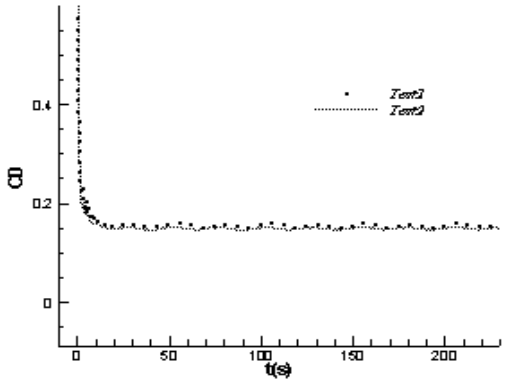

Fig 17. Drag coefficient history of NACA0012 airfoil for rotational- translational motion, cases 1 and 2

6 CONCLUSION

The moving mesh algorithm of Ref. 13 is extended to solve two-dimensional compressible viscous turbulent flow around two bodies in relative motion with respect to each other. Definition of two grid zones has provided the capability of simulating translational and rotational motion of bodies easily. This algorithm is validated on different grid configurations to prove accuracy of interpolation stencil used in this study. The correct performance of algorithm strategy on two sets of grids A and B, sequentially has been demonstrated on various grid configurations. Compressible flow is solved on two moving body benchmark problems, defined in this study, to show capability of the present algorithm in capturing accurate results.

REFERENCES

[1] A.L. Gationde, A Dual-Time for Solution of the Unsteady Navier-Stokes Equation , *Aeronautical J*., 98, pp. 283-291 (1994)

[2] J.T. Batina., Unsteady Navier-Stokes Algorithm with Unstructured Dynamic Mesh for Complex-Aircraft Aerodynamic Analysis , *AIAA Journal*., Vol. 29, No. 3, pp. 327–33, (1991)

[3] H.M. Tsai. and A.S.F. Wong,. et al, Unsteady Flow Calculations with a Parallel Multiblock Moving Mesh Algorithm, *AIAA Journal*, Vol. 39, No. 6, pp.1021-1029 , (2001)

[4] A. Jahangirian , and M. Hadidolabi, An Implicit Solution of the Unsteady Navier-Stokes Equations on Unstructured Moving Grids, *24th International Congress of the Aeronautical Science*, (2004)

[5] J.L. Steger., F.C. Dougherty., and J.A. Benek., A chimera Grid Scheme, Advances in Grid generation, edited by K. N. Ghia and U. Ghia, FED-Vol. 5, *American Society of Mechanical Engineers*, New York, (1983)

[6] J.A. Benek., P.G. Buning,., and J.L. Steger, A 3-D Chimera Grid Embedding Technique, *AIAA* Paper 85-1523, (1985)

[7] K. Nakahashi , F. Togashi, and D. Sharov, Intergrid-Boundary Definition Method for Overset Unstructured Grid Approach, *AIAA Journal*, Vol. 38, No. 11, pp. 2077-2084 ,(2000)

[8] M.J. Aftosmis, M.J. Berger and J.E. Melton, Robust and Efficient Cartesian Mesh Generation for Component-Based Geometry, *AIAA* Paper No. 97-0196, (1997)

[9] S. M. Mirsajedi, S. M. H. Karimian, and M. Mani., A Multizone Moving Mesh Algorithm for Simulation of Flow Around a Rigid Body With Arbitrary Motion, *ASME Journal of Fluids Engineering*, 128, pp. 297-304, (2006)

[10] S. M. Mirsajedi, S. M. H. Karimian, Evaluation of A Two-Dimensional Moving-Mesh Method for Rigid Body Motions , *Aeronautical Journal*, 110(1109), pp. 429-438., (2006)

[11] H. Alisadeghi, H., S. M. H. Karimian, A. Jahangirian, An Implicit Dual Time Stepping Algorithm for Hybrid Dynamic Meshes , Proceedings of 14th *Annual Conference of The Computational Fluid Dynamics*, Canada. (2006)

[12] M. Liou , and C.J. Steffen , A New Flux Splitting Scheme, *Journal of Computational physics* 107, pp. 23-39 , (1993)

[13] F.S. Salehi , and S.M.H. Karimian, Moving Mesh Method for Relative Motion of Two Bodies. *The 7th conference of Iranian Aerospace Society*, Sharif University of Technology,February 19-21,(2008)

[14] A. Jameson , Time-dependent Calculations Using Multi-grid, with Applications to Unsteady Flows Past Airfoils and Wings, *AIAA* Paper No 91-1596, (1991)

[15] A. Jameson ,W. Schmidt and E. Turkel, Numerical Solution of the Navier-Stokes Equations by Finite Volume Methods Using Runge-Kutta Time Stepping Schemes , *AIAA* Paper 81-1259, 1981.

[16] A. Jameson and D. Mavriplis , Finite Volume Solution of the Two Dimensional Navier-Stokes Equation on a Regular Triangular Mesh , *AIAA Journal*, Vol. 24, NO. 4, pp. , (1986)

[17] A. Jameson , Time-dependent Calculations Using Multi-grid, with Applications to Unsteady Flows Past Airfoils and Wings , *AIAA* Paper No 91-1596, (1991)
[18] A. Jahangirian , and M. Hadidoolabi, An Implicit Solution of the Unsteady Navier-Stokes Equations on Unstructured Moving Grids , *24th International Congress of the Aeronautical Science*, (2004)

[19] M. Bristeau, R. Glowinski, J. Periaux, and H. Vivand, Numerical Simulation of Compressible Navier- Stokes Flow, Federal Republic of Germany, Friedr. Vieweg und Sohn,PP.349 , (1987)

[20] Compendium of Unsteady Aerodynamic Measurements, Report No. AGARD-702, 1982

[21] A. Jahangirian, and M. Hadidoolabi, Unstructured Moving Grids for Implicit Calculation of Unsteady Compressible Viscous flow , International Journal for Numerical Methods in Fluids, 47, pp. 1107-1113, (2005)